Study of damage of t-joint components by using different non-destructive techniques

Palumbo, D., De Finis, R., Saponaro, A., Nobile, R., Panella, F., et al.

D. Palumbo, R. De Finis, A. Saponaro, R. Nobile, F. Panella, U. Galietti, "Study of damage of t-joint components by using different non-destructive techniques," Proc. SPIE 11409, Thermosense: Thermal Infrared Applications XLII, 114090F (23 April 2020); doi: 10.1117/12.2558594

SPIE.

Event: SPIE Defense + Commercial Sensing, 2020, Online Only, California, United States

STUDY OF DAMAGE OF T-JOINT COMPONENTS BY USING DIFFERENT NON- DESTRUCTIVE TECHNIQUES

D. Palumbo*[a], R. De Finis[a], A. Saponaro[b], R. Nobile[b], F. Panella[b], U. Galietti[a]
[a] Politecnico di Bari-Dipartimento di Meccanica, Matematica e Management, Via Orabona 4, Bari Italia, 70126; [b]Università del Salento, – Dipartimento di Ingegneria dell'Innovazione, Via per Monteroni, 73100 Lecce.

ABSTRACT

The present research is focused on the use of different non-destructive techniques for detecting damage in CFRP composite structures obtained by an innovative technological process: Automated Fiber Placement. The component was a T-joint stringer adhesively bonded to a skin panel. The aim of the present work is to show the capability of these techniques to provide complementary information for detecting the damage in composites.
Automated Fibre Placement consists in an automatic deposing of prepeg or dry plies on a specific mould. The innovation lies in the possibility to reduce the time of the manufacturing process of large and complex structures by using a robotic arm that contemporary deposes fibre tows and pre-polymerizes them. The resulting products present higher quality in terms of surface finish, internal flaws absent and higher mechanical properties.
The T-joint component tested in the present research was addressed to both static and cyclic tests. After the damage was induced in the material it was performed a qualitative and quantitative study of the damage by using different non-destructive techniques: Thermoelastic stress analysis (TSA), Ultrasound tests (UT) and displacement/strain measurements provided by strain gages.
Processing and post-processing procedures were developed to analyze the data from each tests and finally the comparison of the results allowed a complete characterization and an overview of damage in the component by observing specifically where and when it occurred and how many regions of the component were interested. Finally, dimension, shape and depth where assessed.

Keywords: CFRP, Damage, Thermoelastic Stress Analysis, Strain gages, Ultrasounds

1. INTRODUCTION

Composites present specific mechanical properties due to heterogeneity and anisotropic behaviour associated to a low density that make composites very competitive in different engineering fields. For instance, Aerospace field benefits of the high strength-to-weight ratio specifically for structural applications.
The composite materials, however, can be affected by flaws induced by the technological process or by damage mechanisms during the in-service life. The presence of these flaws of course has a great influence on mechanical properties, specifically on ultimate tensile strength and endurance limit[1,2]. Moreover, the complexity of the damage mechanisms related to stacking sequence, technological process requires specific mathematical model to describe the material behaviour that of course varies from case to case.
The complexity of studying the behaviour of composites, is furthermore increased in case of component or structures. In this field experimental technique represent a useful tool to understand/monitor the damage mechanisms and possibly to quantitatively evaluate damaged regions.
In recent years, the experimental techniques were focused on localisation and characterisation (quantitative and qualitative) of the damage. The strain gages and fiber optics can be applied to the material, on surface or in the inner laminae respectively, and provide a great support specifically for the damage monitoring[3-7]. These techniques provide a local measurement of the strain. However, the issues of the just said techniques are related to the proper positioning of the sensors in order to achieve the correct measurement accuracy and to easily handle the sensors in case of replacement or removal[3,4]. On the other hand, the characterisation of small damaged areas, could require a dense sensor grid.
Thermoelastic stress analysis (TSA) is a contactless, full-field technique that allows surface stress/strain measurements of a component undergoing in-service loading, by simply acquiring the temperature[1,2]. The technique is adopted also as a

Thermosense: Thermal Infrared Applications XLII, edited by Beate Oswald-Tranta, Joseph N. Zalameda, Proc. of SPIE Vol. 11409, 114090F · © 2020 SPIE
CCC code: 0277-786X/20/$21 · doi: 10.1117/12.2558594

non-destructive technique to localise and quantify the damage, in this sense it is useful for in-service monitoring of full-scale components undergoing fatigue loadings [8-13].
The aim of the present work is to compare the capability of the thermoelastic stress analysis in localising and estimating the damage to the other established experimental techniques (ultrasound, strain gages) for a T-joint CFRP. The T-joint panel were addressed to fatigue loading under displacement control. TSA exhibited a great capability in detecting when and where damage occurred compared to strain gages. The capability of TSA in determining the extension of damaged area was assessed compared to UT technique performed at the end of the fatigue test.

2. THEORY: THERMOELASTIC STRESS ANALYSIS (TSA)

When a material undergone a cyclic load in the material two kinds of heat sources develop: thermoelastic and dissipative heat sources. The first are reversible and are related to the thermoealstic effect that appears due to cyclic loading, while the second are related to the irreversible thermodynamics processess occurring in the material in presence of damage mechanisms such as: inelastic/anelastic behaviour, viscos-elastoplastic processes, friction made by rubbing surfaces[1,2,14,15].
In presence of adiabatic conditions, the thermoelastic signal for a non-isotropic material is correlated to stress changes in the principal material directions.

$$\Delta T_{el} = -\frac{T_0}{\rho C_p}\left(\alpha_1 \Delta\sigma_1 + \alpha_2 \Delta\sigma_2\right) \tag{1}$$

where α_1 and α_2 are the linear heat expansion coefficients while C_p is the specific heat at constant pressure and ρ the density and T_0 the absolute temperature and $\Delta\sigma_1$ and $\Delta\sigma_2$ are the stresses in the principal directions. Generally, the thermoelastic stress analysis allows obtaining an uncalibrated thermographic signal proprtional to the peak-to-peak stress changes varying sinusoidally due to imposed load. By representing the signal S as a vector, the modulus is the amplitude of thermoelastic signal while the phase shift φ measures the delay between the thermoelastic signal and the reference signal [2]:

$$A^* S = \left(\alpha_1 \Delta\sigma_1 + \alpha_2 \Delta\sigma_2\right) \tag{2}$$

where A is the calibration constant.
In the time domain the thermoelastic signal variation can be represented by the following equation:

$$s = \frac{S}{2}\sin(\omega t + \pi + \varphi) \tag{3}$$

where s is the uncalibrated thermographic signal while ω is the system pulsation.

3. MATERIAL, EXPERIMENTAL SETUP

3.1 Material and Technological process

The automated fiber placement (AFP) is a technological process where unidirectional tows of prepeg are deposed on a mould in a automated process[16-18]. The robot presents seven degrees of freedom to depose the prepeg. The robot presents a pressure roller that applies the correct pressure to compact the tow on the mould. Moreover, it also provides the energy for realising an initial stage of resin polymerisation (figure 1a).

The adopted material is a T-joint panel of CFRP composed by sixteen layers, the layup is $[0/-45/45/90/90/45/-45/0]_2$. The component is a flat panel with a bonded T-stringer, figure 1b. As represented in figure, on the stringer there were applied holes in order to fix the component on the loading machine grips and to uniform transfer the load to the component.

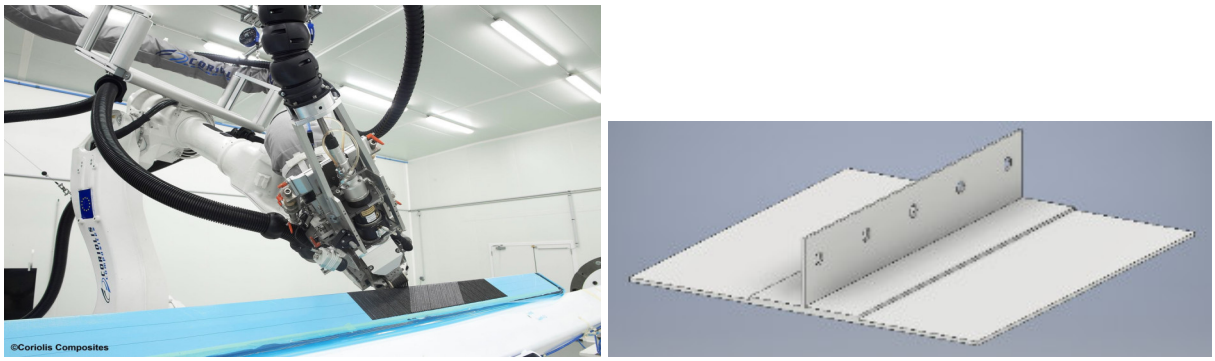

(a) (b)

Figure 1. AFP Robot made by Coriolis ® (a) 3D rendering of the component (b).

3.2 Experimental Setup: strain gages.

On the component, in total ten strain gages were installed on aeronautical component (figure 2b). The acquisition system of the signal from strain gages is the HBM Quantum X, the setup of gages on surface is represented in figure 2a. The adopted strain gages are of the same type self-compensed with a grid length of 6 mm and an electrical resistance of 350 Ω and a gage factor of 2.155±0.5%.

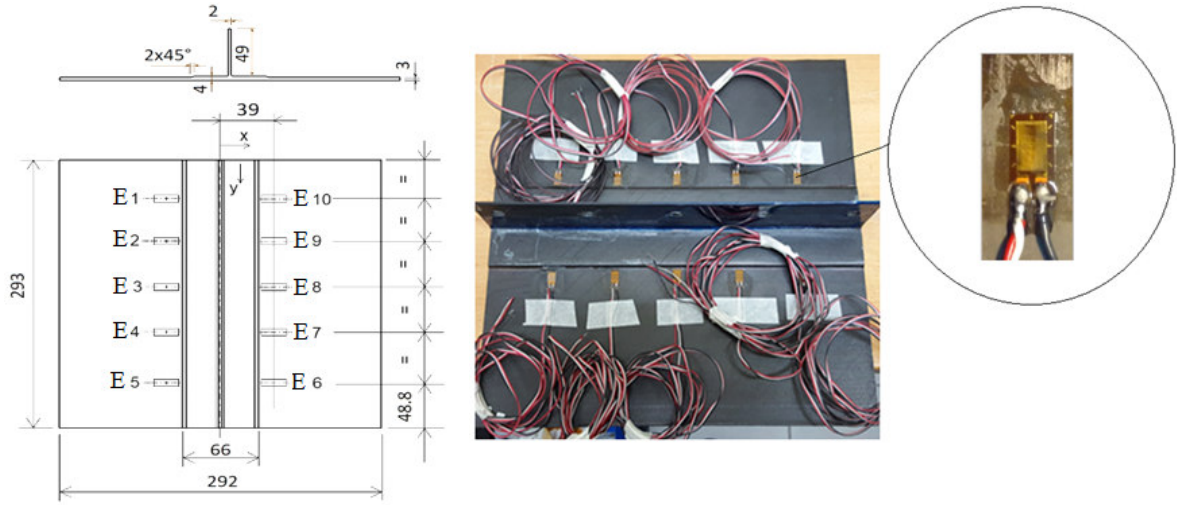

(a) (b)

Figure 2. Setup of strain gages on surface (a); Component and strain gages (b).

The software for analysing the results is CatMan Easy that requires an initialisation of strain gages characteristics, electrical bridge and calibration. It converts the electrical signal in the signal of deformation. Moreover, sampling frequency and supply voltage have to be defined. In this case, the sampling frequency was 75 Hz and the voltage were 2.5V.

3.3 Experimental Setup: Ultrasound (US)

Phased array system consists in a probes matrix that physically use progressive waves, opportunely coordinated and shifted each other's.

The wave-front generated by each element of the array at slightly different times combines with the impulses of the other elements to direct and shape the beam, in order to obtain a sharp focus and a different beam direction[19-20].

The Olympus OmniScan MXU was used for performing the ultrasounds analysis with the phased array (PA). It is equipped with an innovative probe of 64 elements (2.25L64-A2) that presents a frequency of 2.25 MHz. The probe is fixed on a plexiglass wedge. In order to perform the C-scan scanning it was used a Mini-wheel Absolute Encoder with a 12steps/mm of resolution that is connected to the probe to acquire a syncronised data acquisition from the unidirectional moving probe. The scans can be visualised as C-scan maps, by using a suitable 2D data of the investigated surface of the component in XY coordinates. The measuring system is composed by the plexiglass wedge and the encoder, that are fixed on a thermoplastic holder moved along unidirectional path by an aluminium profile (figure 3a and figure 3b) [21] .

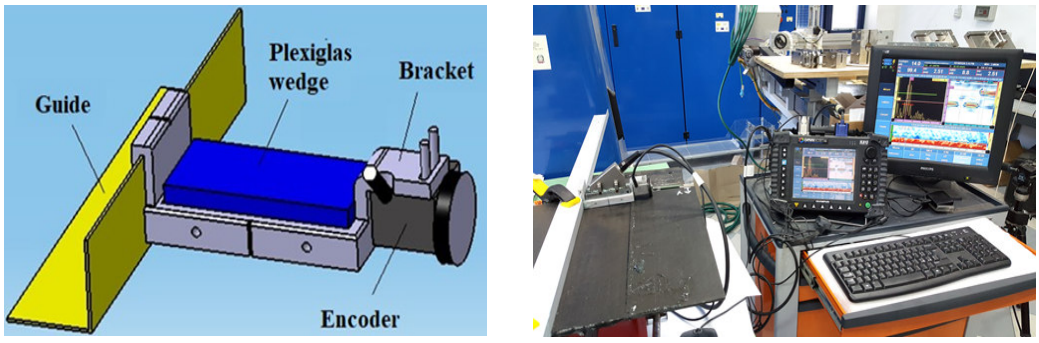

(a) (b)

Figure 3. UT experimental Set-up (a); moving system for the probe (b).

In figure 4, the map of scanned region is represented. In figure are also represented the C-scan directions on the panel: parallel direction ed orthogonal direction to the stringer. The measures from the origin of the reference system are referred to the centre of UT probe.

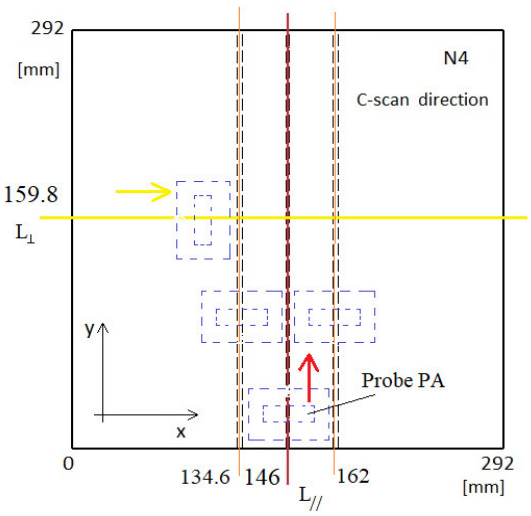

Figure 4. Maps and scanning directions on T-joint panel.

3.4 Experimental Setup: Thermoelastic Stress Analysis (TSA)

The component was addressed to cyclic tests. The load was applied on web of the panel while the panel was constrained in a specific loading system reported in Figure 5 that was fixed in the loading frame. The loading frame was a servo hydraulic Instron 8850 with capacity of 250 kN. The load was applied under displacement control in a stepwise mode were different displacement levels were assigned to the sample. The loading levels were reported in Table I, in terms of mean displacement, displacement semi amplitude and displacement amplitude.

Infrared detector was positioned in front of the sample, the detector was a cooled made by FLIR series X6540 SC, with a 640*512-pixel array and a noise equivalent temperature difference less than 30 mK. The thermal sequences were acquired at a frequency of 177 Hz. For each loading level of Table I, there is the related thermal sequence acquired.

Figure 5. Experimental setup for TSA tests

Table 1. Imposed displacement levels

Level	Smed [mm]	$\frac{\Delta S}{2}$ [mm]	ΔS [mm]
1	1.90	0.80	1.60
2	2.25	0.95	1.90
3	2.81	1.19	2.38
4	3.38	1.42	2.84
5	3.94	1.66	3.32
6	4.50	1.90	3.80

Thermal sequences were processed according the analysis provided in [1]. The algorithm for the signal reconstruction is described in Eq. 4 where *Sm* is the signal and provides pixel by pixel all the information on its components:

$$S_m(t) = S_0 + at + S1\sin(\omega t + \varphi) + S2\sin(2\omega t) \quad (4)$$

where $S_0 + at$ is the mean temperature, S_1 and φ are the amplitude and phase shift of the thermoelastic signal and S_2 is the amplitude of second order harmonics related to dissipative processes[22-24].

Present research refers to the analysis of S_1 parameter opportunely normalized by the displacement amplitude (Table 1) as an indicator of damaged area through fatigue cycles.
In figure 6 the algorithm is schematically represented in order to quantitively estimating the debonding.

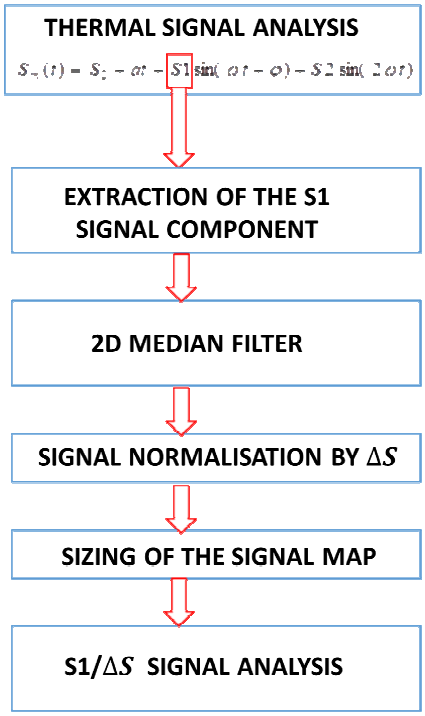

Figure 6. Algorithm of thermoelastic data analysis

4. RESULTS

4.1 Strain gages

In Figure 7a, are reported for all the strain gages the deformation variations ($\Delta\varepsilon = \varepsilon_{max} - \varepsilon_{min}$) normalised by imposed displacement amplitude (ΔS) as a time dependent function for all the displacement level imposed. Referring to the results for the first load level, the $\Delta\varepsilon/\Delta S$ exhibits a low variability that remains roughly constant throughtout the load levels. After about 4000 s, at the fifth displacement level, it is observed by all the strain gages a deformation reduction. Only strain gage E1 exhibits a strain reduction (from 748 με to 693 με) in advance if compared to the other sensors.
A more accurate examination of the strain measurements can be performed by considering mean strain normalised by the displacement amplitude, figure 7b.
From the curves of figure 7b, it is observed that the deformation is still constant up to $\Delta S = 2.38$ mm and it starts to reduce in the following steps. At a $\Delta S = 3$ mm the curves show a severe decrease of deformation due to the incoming debonding on each side of the T-joint.
The strain gage E1 presents strain values lower than others with a decreasing in the strain in advance with respect to the other gages. This is in accordance with Figure 7a. This can be explained by the fact that the E1 was setup on the edge where possibly the debonding started firstly. The gages E7-E6 installed on right side of the panel (Figure 2a) exhibit higher values of strain than E8-E9 on the same edge. Strain gages E4-E5 read a lower strain values in the same way as E3-E2 gages. This demonstrates as the right side of the panel is greatly damaged.

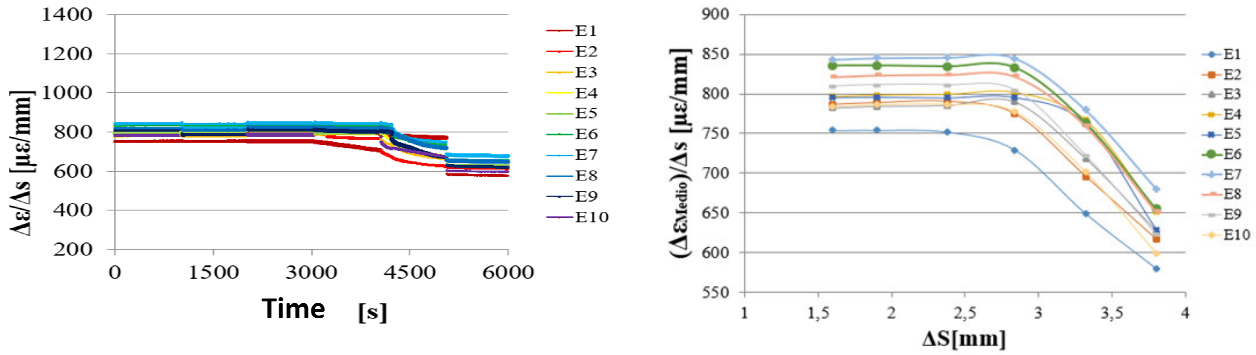

(a) (b)

Figure 7. time-dependent behaviours of $\Delta\varepsilon/\Delta s$ (a) and $\Delta\varepsilon_{Medio}/\Delta s$ (b).

4.2 Ultrasounds

From ultrasound probes it results that there are debonding on both sides of the bonded region of the T-joint. The damage is symmetric while in central regions of the bond skin-to-web any damage results.

In figure 8a it was presented a map of C-scan on the panel at 2.36 mm of depth on the left side of the stringer. The debonding detected presents a non-uniform damaged area of 8 mm on the total length of the panel.

In figure 8b, the right side of the panel is represented in the C-scan maps. In this case the debonding is uniform and presents an extension of 10 mm.

No further damage was detected in the inner part of the skin by varying the depth of C-scan.

In figure 9a, the C-scan map at 5.28 mm of depth (UT signal of background echo) in the central part of the stringer where no damage was observed. The UT scan in the skin (figure 9b) in the central region do not show any damage.

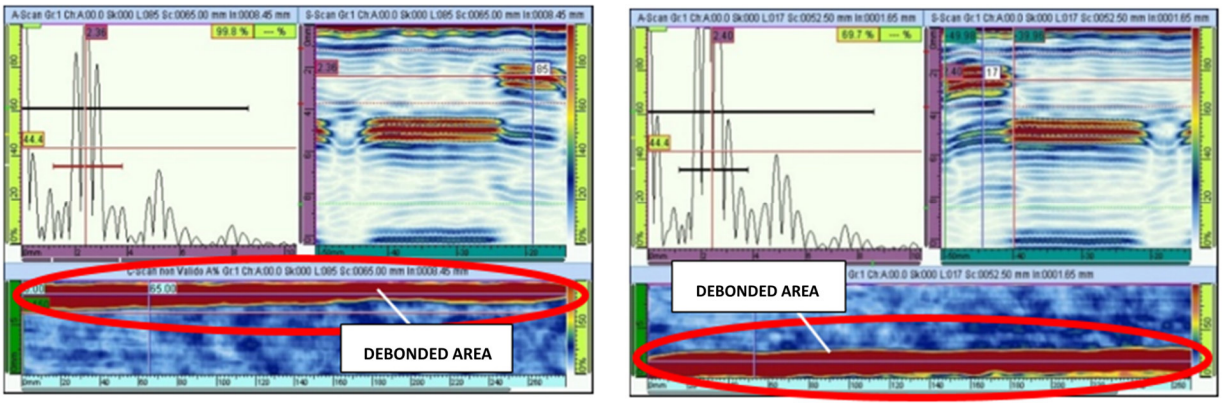

(a) (b)

Figure 8. UT scansion of the panel: left side (x=134.6 mm) (a) and right side (x=162 mm) (b).

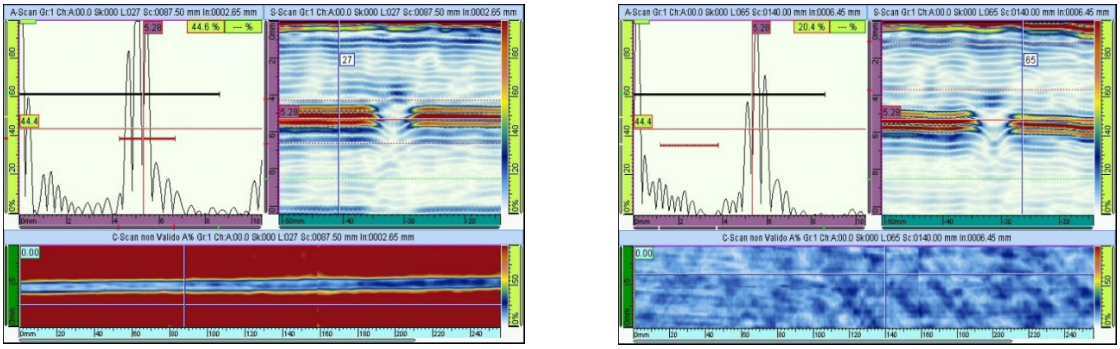

(a) (b)

Figure 9. C-scan map central part at x= 146 mm: stringer (a) and skin (b).

In order to characterise the damage, a reference criterion was established: it was fixed a threshold in the A-scan of the 60%. The peak of the UT signal due to debonding was of the 100% hence 40% higher than defined threshold. In table 2 the results of the UT investigations were reported coupled with an estimation of debonded area (Δsdeb.).

Table 2: Resume of UT investigation and debonded area

Component	**Position [mm]**		**Direction C-scan**	**Depth C-scan [mm]**	**Gain [dB]**	**$\Delta s_{deb.}$ [mm]**	**Bonded area [mm^2]**
	x	y					
N4	134,6	0	Left side	2,36	14	8	14064
	162	0	Right side	2,36	14	10	
	146	0	Central region	≈5	14		NO damage

4.3 Thermoelastic Stress Analysis

As previously explained, the thermoealstic signal was used as parameter to estimate the damage.
Firstly, a reference area, sound area, for the analysis was determined. Specifically, there were individuated three areas: in the central part of the stringer (area C), and at left and right sides of the stringer, respectively A-B areas, as reported in figure 10. The signal *S1/ΔS* from these areas was evaluated for each load level of the test. In particular, by observing the figure, a signal reduction characterising the three area is present.
In figure 11, quantitative data of maximum/minimum/mean values of *S1/ΔS* reveal that there is an initial phase of signal stabilisation through the loading and a decrease of *S1/ΔS* in the last part of the test. This behaviour is characteristic of area A-B-C. The final decrease of the signal can be ascribed to a reduction of loading bearing capability as the stringer debonding occurs. Moreover, as the debonding occurs, the material experiences a stiffness reduction.
In general, the debonding process for the present panel is not uniform, there will be areas bonded and areas debonded, but the overall behaviour is characterised of course by a global stiffness reduction. This explains the signal reduction even in those area that area bonded.
To obtain a quantitative evaluation of the debonded area, the analysis of the mean values of *S1/ΔS* in the three chosen areas was performed. This lead to fix a threshold to separate damaged from undamaged areas. The threshold adopted was the mean value of *S1/ΔS* of the A-B areas plus the standard deviation of the data in the same areas.
By comparing the value of each pixel to the threshold, it is possible to assess a binarised map, figure 12, that leads to estimate damaged area.
By simply observing figure 12 a quantitative comparison of bonded area between different loading levels is possible. By increasing the displacement level, of course the debonded area increases. The assessment of the number of pixels out of threshold lead to a quantitative estimation of debonded area. The damaged area was considered as the debonded area normalised by the nominal area.

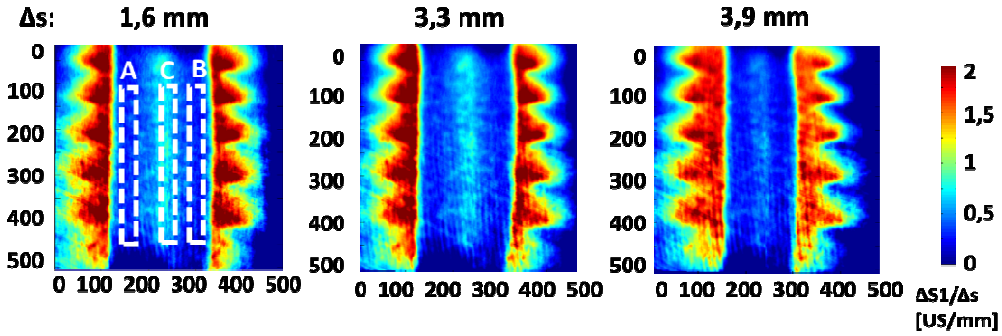

Figure 10. S1/ΔS maps for different loading levels

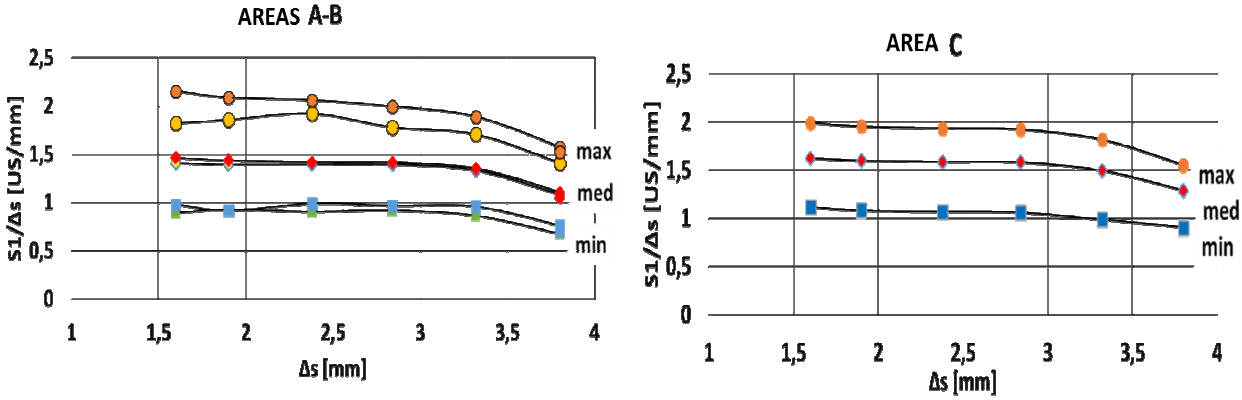

Figure 11. threshold values of S1/ΔS for different loading levels in areas A-B-C.

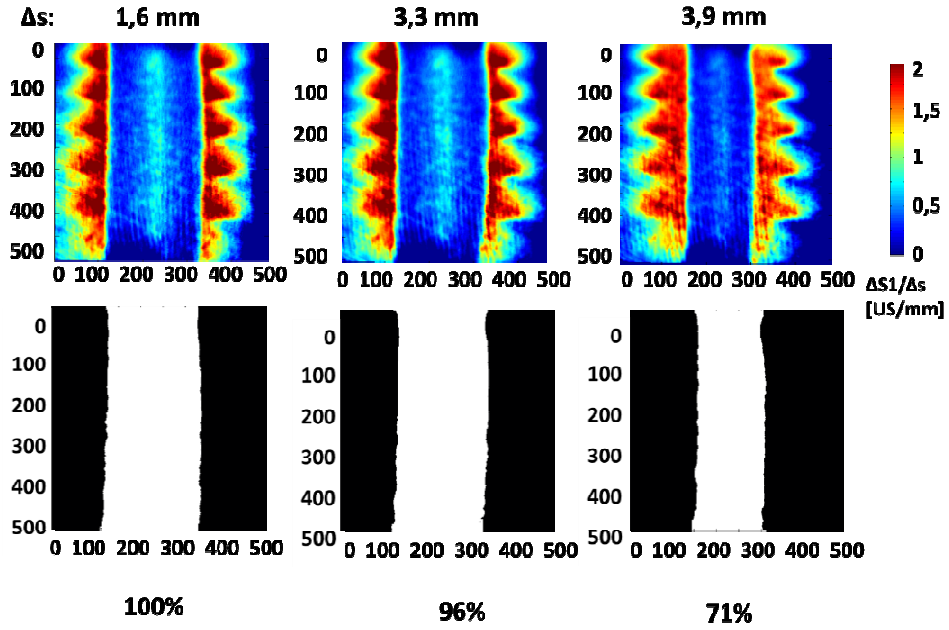

Figure 12. Binarisation of thermoelastic maps to obtain debonded area.

5. DISCUSSION

The results presented in previous sections show that the thermoealstic technique is capable of evaluating when and where damage occurs and possibly providing a quantitative estimation of debonded area.
The thermoelstic signal, is specifically in very good agreement with the results provided by strain gages. In effect the significant thermoelastic signal reduction occurs at the same load amplitude as the strain decrease, in correspondence of the stringer debonding. Due to full field map, it is possible to quanitify locally, pixel by pixel the amount of damage, without stopping the test.
The amount of debonded area was performed by counting the pixel over the threshold, figure 12. In particular, it was observed that in the first loading step (ΔS=1,6 mm) the area was roughly similar to nominal area, 18496 mm^2 (100% of nominal area), it means that no damage was present. In the loading level three, at ΔS=3,3 mm, the area reduction due to debonding of the stringer was about 4%, it means that the measured area was the 96% of the nominal area. Finally, at the loading level, ΔS=3,9 mm the measured area was of 13712 mm^2 and the debonded area was roughly the 30% of the nominal area. This last result can be compared to UT tests that were performed after the fatigue test. In effect, the debonded area obtained by thermoelastic map matched the area measured by UT with an error less than 1%.

6. CONCLUSIONS

In the present work, the thermoelastic stress analysis technique (TSA) was adopted for the damage evaluation of a T-joint CFRP panel obtained by Automated Fiber Placement.
The panel was subjected to stepwise cyclic loading under displacement control.
The thermoelastic signal results were compared to the results provided by well-established technique: strain gages and UT.
The thermoelastic stress analysis demonstrated great capability in detecting quantitatively and qualitatively the amount of debonded area. Moreover, the time instant at which damage initiated can be assessed.
TSA with respect to UT and strain gages, allows continuous measurements and analysis and full field maps of the areas undergoing cyclic load. This is particularly advantageous for the in-service monitoring of structural components where it is not feasible to apply strain gages or to perform UT tests.

REFERENCES

[1] De finis R., Galietti U., “Fatigue behaviour assessment of automated fiber placement composites by adopting the thermal signal analysis”, in: 2019 Proceedings of SPIE - The International Society for Optical Engineering 11004,110040H.
[2] Palumbo, D., De Finis R., Demelio, GP., and Galietti U., “Study of damage evolution in composite materials based on the Thermoelastic Phase Analysis (TPA) method”. Composite Part B, 117, 49-60, (2017).
[3] Güemes, A. Fernández-López, P. F. Díaz-Maroto, A. Lozano, J. Sierra-Perez, “Structural Healt Monitoring in Composite Structures by Fiber-Optic Sensors”, *Sensors*, 18, 1094 (2018).
[4] R. Di Sante, “Fibre Opric Sensors for Structural Health Monitoring of Aircraft Composite Structures: Recent Advances and Applications”, Sensors, 15, 18666-18713 (2015).
[5] I. Herszberg, H. C. H. Li, F. Dharmawan, A. P. Mouritz, M. Nguyen, J. Bayandor, “Damage assessment and monitoring of composite ship joints”, *Composite Structures*, 67, 205-216 (2005).
[6] Ruzek, R., Kadlec, M., Tserpes K., and Karachalios E. “Monitoring od compressive behaviour od stiffened composite panels using embedded fibre optic and strain gauge sensors”, *International Journal of Structural Integrity*, 8 (1), 134-150 (2017).
[7] Baskar Rao, M., Bhat, M.R., Murthy, C. R. L., Venu Manhav, K., and Asokan S., “Structural Health Monitoring (SHM) Using Strain Gauges, PVDF Film and Fiber Bragg Grating (FBG) Sensors: A comparative Study”, Proc. National Seminar on Non-Destructive Evaluation, 7-9 December, 2006, Hyderabad.

[8] Freire, J. L. F., Waugh, R. C., Fruehmann, R. , Dulieu-Barton, J. M. "Using Thermoelastic Stress Analysis to Detect Damaged and Hot Spot Areas in Structural Components", *Journal of Mechanics Engineering and Automation*, 5, 623-634 (2015).
[9] Earl, J. S. , Dulieu-Barton, J. M., Shenoi, R. A.. "Determination of hygrothermal ageing effects in sandwich construction joints using thermoelastic stress analysis", *Composites Science and Technology*, 63, 211-223 (2003).
[10] Freuhmann, R. K. , Dulieu-Barton, J. M., Quinn, S., Peon-Walter, J., Mousty, P. A. N. "The application of thermoelastic stress analysis to full-scale aerospace structures", *Journal of Physics: Conference series*, 382, 012058 (2012).
[11] Rajic,N., Brooks, C., Wang, J., Forrester, C., Swanton, G. "Thermoelastic Stress Analysis for Structural Performance Assessment of Aerospace Composites", 21st International Conference on composite Materials, Xi'an, 20-25 August, 2017.
[12] Sakagami, T., Izumi, Y., Shiozawa, D., Fujimoto, T., Mizokami, Y. , Hanai, T. "Nondestructive Evaluation of Fatigue Cracks in Steel Bridges Based on Thermoelastic Stress Measurement", 21st European Conference on Fracture, ECF21, 20-24 June, 2016, Catania, Italy.
[13] Rajic,N., Galea,S. "Thermoelastic stress analysis and structural health monitoring: An emerging nexus", *Structural Health Monitoring*, 14, 52-72, 2014.
[14] Montesano, J. , Fawaz, Z., Bougherara, H. "Use of infrared thermography to investigate the fatigue behavior of a carbon fiber reinforced polymner composite". Composite Structures, 97,76-83 (2013).
[15] Pierron,f., Green, B., Wisnom, M.R.. "Full-field assessment of the damage process of laminated composite open-hole tensile specimens, Part I: methodology". Composites Part A 38, 2307–20 (2007).
[16] Belnoue, J.P.H. and Mesogitis, T. "Understanding the buckling behaviour of steered tows in Automated Dry Fibre Placement (ADFP) placement pre-preg laminates". Composites: Part A 102, 196–206 (2017).
[17] Schmidt, C., Denkena B. et al. "Thermal image-based monitoring for the automated fiber placement process". 10th CIRP Conference on Intelligent Computation in Manufacturing Engineering - CIRP ICME, 2016.
[18] Lichtinger, L., Hörmann P., Stelzl D., Hinterhölzl, R. "The effects of heat input on adjacent paths during Automated Fibre Placement". Composites: Part A 68, 387–397 (2015).
[19] Dattoma, V., Nobile, R., Panella, F.W., Pirinu, A., Saponaro, A., "Optimization and comparison of ultrasonic techniques for NDT control of composite material elements", Proceedings of AIAS 2018, Villa San Giovanni/Italy, September 2018, Vol. 12, 9-18;
[20] Dattoma, V., Panella, F.W., Pirinu, A., Saponaro,A. "Advanced NDT Methods and Data Processing on Industrial CFRP Components", Applied Sciences, 2019, Vol. 9, 3, 1-17;
[21] Bulavinov A., Kröning M., Pudovikov S., Oster R., Hanke R., Hegemann U., Reddy K. M., Venkat R. S.: "Application of Sampling Phased Array Technique for ultrasonic inspection of CFRP components". International Symposium on NDT in Aerospace, Berlin, 2008, 21-38.
[22] De Finis, R., Palumbo, D., Galietti, U. "Fatigue damage analysis of composite materials using thermography-based techniques" Procedia Structural Integrity 18,. 781-791 (2019)
[23] De Finis R, Palumbo D, Galietti U, A Multianalysis Thermography-Based Approach For The Fatigue And Damage Investigation Of Astm A182 F6nm Steel At Two Stress Ratios. Fatigue and Fracture of Engineering materials and structures. Fatigue and Fracture of Engineering Materials and Structures 42(1), pp. 267-283, 2019.
[24] De Finis R, Palumbo D, Ancona F, Galietti U, (2017), Fatigue Behaviour of Stainless Steels: A Multi-parametric Approach, Residual Stress, Thermomechanics & Infrared Imaging, Hybrid Techniques and Inverse Problems, Volume 9, Proceedings of the 2016 Annual Conference on Experimental and Applied Mechanics, pp. 1-8, ISBN: 978-3-319-42254-1, DOI: 10.1007/978-3-319-42255-8_1.